

Nonlinear Multi-Carrier System with Signal Clipping: Measurement, Analysis, and Optimization

Yuyang Du, *Graduate Student Member, IEEE*, Liang Hao, *Member, IEEE*,
Yiming Lei, *Member, IEEE*, Qun Yang, *Student Member, IEEE*, Shiqi Xu, *Student Member, IEEE*,

Abstract—Signal clipping is a well-established method employed in orthogonal frequency division multiplexing (OFDM) systems to mitigate peak-to-average power ratio (PAPR). The utilization of this technique is widespread in electronic devices with limited power or resource capabilities due to its high efficiency and low complexity. While clipping effectively diminishes nonlinear distortion stemming from power amplifiers (PAs), it introduces additional distortion known as clipping distortion. The optimization of system performance, considering both clipping distortions and the nonlinearity of PAs, remains an unresolved challenge due to the intricate modeling of PAs. In this paper, we undertake an analysis of PA nonlinearity utilizing the Bessel-Fourier PA (BFPA) model and simplify its power expression through inter-modulation product (IMP) analysis. We mathematically derive expressions for the receiver signal-to-noise ratio (SNR) and system symbol error rate (SER) for nonlinear clipped OFDM systems. By means of these derivations, we explore the optimal system configuration required to achieve the lower bound of SER in practical OFDM systems, taking into account both PA nonlinearity and clipping distortion. The results and methodologies presented in this paper contribute to an improved comprehension of system-level optimization in nonlinear OFDM systems employing clipping technology.

Index Terms—Signal Clipping, OFDM, Nonlinear Distortion, Power Amplifier

I. INTRODUCTION

Power amplifiers (PAs) exhibit nonlinear characteristics when faced with high-power input signals, which is commonly referred to as PA nonlinearity [1]–[8]. The rapid progress of multiple-input and multiple-output (MIMO) technology, coupled with the growing number of subcarriers, has resulted in a significant rise in the peak-to-average power ratio (PAPR) of orthogonal frequency division multiplexing (OFDM) devices. This increase in PAPR poses a major challenge in practical OFDM systems, as it can lead to reduced power efficiency, degraded system performance, and potential distortion in the transmitted signals. PA's nonlinearity has become a vital concern, as it may cause significant performance degradation when faced with high PAPR [9], [10]. To ensure system linearity, designers are compelled to reduce the input power of the amplifier, albeit at the cost of energy efficiency [11]. Reducing PAPR, as a result, has emerged as a critical problem in OFDM systems and has attracted significant research attention.

Several established PAPR reduction algorithms [12]–[15] have been extensively studied. However, these conventional al-

gorithms, such as partial transmit sequence (PTS) and selected mapping (SLM), involve complex signal processing, making them unsuitable for resource-limited or battery-driven devices, which is common in sensors and Internet of Things networks.

Signal clipping offers a less complex PAPR reduction approach [16]–[18]. In OFDM systems, clipping is realized in the time-domain signals to limit their magnitude to a predetermined threshold. This approach effectively limits the PAPR of OFDM signals within an upper bound with relatively small computation requirements and is therefore very popular in resource-constrained OFDM devices [19]. However, as a nonlinear operation, signal clipping introduces additional frequency components that never appear in the original signal, bringing both out-of-band radiation and in-band distortion to the original signal. Although radiation spilling beyond the target bandwidth can be restricted by filtering, how to deal with the in-band distortion is still a challenging problem.

Prior research has made efforts to investigate and mitigate the in-band distortion caused by signal clipping. In [20], a novel Bayesian approach was implemented to recover the clipped signals of an OFDM system, aiming to minimize the impact of in-band distortion at the receiver side. Another technique, proposed in a separate publication [21], is known as the repeated clipping and filtering (RCF) method. The RCF technique focuses on reducing distortion on individual tones of the OFDM signal. Researchers have also explored optimization techniques to enhance the performance of signal clipping for PAPR reduction in OFDM systems. In a couple of studies [22], [23], the authors optimized both the clipping and filtering stages to achieve improved PAPR reduction while simultaneously mitigating in-band distortion. Alternative approaches have been investigated to tackle the computational complexity associated with clipped OFDM systems. For example, [24] applies convolutional neural networks (CNN) to reduce computational complexity while maintaining PAPR reduction performance. Additionally, compressed sensing techniques were employed in another study [25] to recover the signal clipping noise in clipped OFDM signals.

However, the joint impact of PA nonlinearity and clipping distortion has received little attention in previous studies. Intuitively, the choice of clipping level introduces a trade-off between PA nonlinearity and clipping noise: a higher clipping level reduces PA nonlinearity but increases clipping noise, while lower clipping levels decrease clipping noise but amplify nonlinear distortion. A previous research [26] tried to understand the problem via simulations. However, the complex settings in real-world engineering scenarios necessitate a *theoretical* analysis of the trade-off between these two distortion sources. Otherwise, with simulations only, we are unable to

Y. Du and Y. Lei are with the School of Electronics, Peking University, Beijing, China. H. Liang is with 2012 Laboratory, Huawei Technologies Co., Ltd, Beijing, China. Q. Yang is with the Department of Information Engineering, The Chinese University of Hong Kong, Shatian, Hong Kong SAR. S. Xu is with the School of Electronics and Information Technology, Sun Yat-sen University, Guangdong, China. An early version of this paper [1] has been presented in IEEE VTC2023.

comprehensively understand the problem, let alone optimize the system setting to achieve the best performance.

In light of this, the primary objective of this paper is to thoroughly investigate the trade-off between clipping distortion and PA nonlinearity in practical OFDM systems and make optimizations accordingly. By addressing this trade-off, we aim to enhance the overall system performance and mitigate the adverse effects of both clipping distortion and PA nonlinearity. The contributions of this research can be summarized as follows:

- To simplify the representation of PA nonlinearity, we utilize the Bessel-Fourier PA (BFPA) model. Through an analysis of the inter-modulation product (IMP) in the PA's output, we derive the signal-to-noise ratio (SNR) for the studied system, where both nonlinear PAs and signal clipping are taken into consideration.
- Our optimization problem is approached from three distinct scenarios. In the first scenario, we consider a known power level for the PA's nonlinear distortion. By deriving the optimal clipping level, we aim to minimize the symbol error rate (SER). Moving on to the second scenario, we assume the power of clipping distortion is known. In this case, we derive the optimal operating point for the PA that minimizes the SER. Lastly, we address the scenario where both PA nonlinearity and clipping distortion are unknown variables. We prove the existence of a global minimum SER and derive the optimal signal clipping level and PA operating point. Besides, we obtain a closed-form expression for the global SER lower bound, which enhances our understanding of the system's performance.
- We thoroughly examine the impact of various system parameters on both the SER and total degradation (TD) in the presence of signal clipping noise and PA nonlinearity. Our investigation offers a comprehensive analysis of how these system parameters contribute to the overall performance degradation.

This paper is organized as follows. Section II presents the framework of the studied nonlinear clipped OFDM system. Section III-A builds the BFPA model, Section III-B analyzes the PA nonlinear distortion, and Section III-C derives the closed-form expression of SER. Then in Section IV, SER optimizations with different constraints are presented in detail. Section V gives simulation results and explains our experimental observations. Section VI concludes this paper.

This paper uses the following notation conventions. we denote matrices by bold capital letters, e.g., \mathbf{M} . And we denote the element of a matrix and the conjugate of the element by $[\mathbf{M}]_{i,j}$ and $[\mathbf{M}]_{i,j}^*$, respectively. We represent the Frobenius norm of a matrix by $\|\mathbf{H}\|_F$. We denote the expectation operator and the variance operator by $E(\cdot)$ and $Var(\cdot)$, respectively. Furthermore, $\mathcal{CN}(m, \sigma^2)$ represents a complex Gaussian random variable with a mean of m and a variance of σ^2 .

II. SYSTEM MODEL

We first present the general framework of the studied system in Fig. 1. The number of subcarriers is denoted as N_S .

Additionally, the system we considered is comprised of N_R receive antennas and N_T transmit antennas. We then represent the source bit stream by vector \mathbf{U} and denote the output of the M -order Quadrature Amplitude Modulation (M-QAM) modulator by matrix \mathbf{M} . Further, the modulated symbol transmitted through the t^{th} transmitter antenna (where $t = 1, 2, \dots, N_T$) during the s^{th} time slot (where $s = 1, 2, \dots, N_S$) is denoted as $[\mathbf{M}]_{t,s}$.

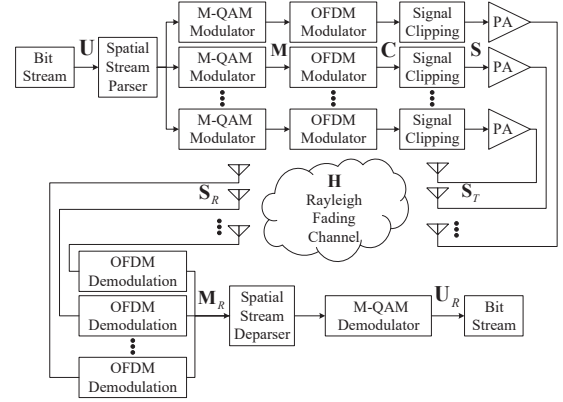


Figure 1. The framework of the investigated OFDM system incorporates both a nonlinear PA and signal clipping.

We make an assumption that the inverse fast Fourier transform (IFFT) module has a length N_S , which is equal to the number of subcarriers. Consequently, the signal obtained after the OFDM modulator can be expressed as

$$\mathbf{C} = \mathbf{M}\mathbf{E}^+ \quad (1)$$

where \mathbf{E}^+ represents the IFFT operation within the OFDM modulation. The (k, s) element within the matrix can be written as [27]

$$[\mathbf{E}]_{k,s}^+ = e^{j2\pi(s-1)(k-1)/N_S} \quad (2)$$

We define the system input power as E_U , which represents the system operating point. Additionally, we denote the input power of the signal clipping blocks as E_C . Furthermore, at the t^{th} transmit antenna, the s^{th} post-IFFT symbol transmitted is denoted by $[\mathbf{C}]_{t,s}$. The expression for E_U can be written as

$$E_U = \frac{\sum_{x=1}^{N_T N_S} E([\mathbf{U}]_x [\mathbf{U}]_x^*)}{N_S} = \frac{\sum_{t=1}^{N_T} \sum_{s=1}^{N_S} E([\mathbf{C}]_{t,s} [\mathbf{C}]_{t,s}^*)}{N_S} \quad (3)$$

We then express the output signal of the clipping module as

$$[\mathbf{S}]_{t,s} = \begin{cases} [\mathbf{C}]_{t,s}, & \text{when } [\mathbf{C}]_{t,s} \leq \eta\sqrt{E_U} \\ \eta\sqrt{E_U}e^{j\angle[\mathbf{C}]_{t,s}}, & \text{otherwise} \end{cases} \quad (4)$$

where the phase of the transmitted symbol is denoted by $\angle(\cdot)$, and the signal clipping level is represented by η . From (4), we see that the output power of the clipped signal is upper-bounded by $\eta^2 E_U$.

Building upon Equation (4), the scaling factor β for signal power is written as,

$$\beta = \eta \int_{\eta}^{\infty} e^{-t^2} dt + 1 - e^{-\eta^2} \quad (5)$$

We then write the signal matrix after clipping as

$$\mathbf{S} = \mathbf{D}_{clip} + \beta \mathbf{C} \quad (6)$$

where \mathbf{D}_{clip} denotes the signal clipping distortion, and we have $\mathbf{D}_{clip} \sim G(0, D_k E_U)$.

We write the coefficient of clipping distortion power as

$$D_k = \frac{1}{J} FFT\{\mathbf{S}\}_k - \beta^2 / (1 - e^{-\eta^2}) \quad (7)$$

where the over-sampling factor is written as J , and the k^{th} output of the JN -point fast Fourier transform (FFT) is denoted by $FFT\{\}_k$.

The power of the signal clipping module's output can be expressed as

$$E_S = \frac{1}{N_S} \sum_{t=1}^{N_T} \sum_{s=1}^{N_S} E\left([\mathbf{S}]_{t,s} [\mathbf{S}]_{t,s}^*\right) = D_k E_U + \beta^2 E_U \quad (8)$$

As in Fig. 1, we represent the input of nonlinear PAs by \mathbf{S} , which is the clipped output of prior modules. And we represent the output symbol of PA by \mathbf{S}_T , which is expressed as

$$\mathbf{S}_T = \alpha \mathbf{S} + \mathbf{D}_{non} = \alpha \beta \mathbf{C} + \alpha \mathbf{D}_{clip} + \mathbf{D}_{non} \quad (9)$$

where \mathbf{D}_{non} represents the nonlinear distortion of amplifiers and α denotes the PA's linear gain factor.

Radio-frequency signals received at the receiver antenna can be written as

$$\mathbf{S}_R = \mathbf{H} \mathbf{S}_T + \mathbf{D}_{ch} \quad (10)$$

where the channel noise is represented by \mathbf{D}_{ch} , and the uncorrelated elements of \mathbf{D}_{ch} can be written as $\mathcal{CN}(0, \sigma_{ch}^2)$. Further, the quasi-static Rayleigh channel applied in the system is denoted by \mathbf{H} .

The output signal of the FFT module (i.e., the OFDM demodulator) is expressed as

$$\mathbf{M}_R = \mathbf{S}_R \mathbf{E}^- = (\alpha \mathbf{H} \mathbf{S} + \mathbf{H} \mathbf{D}_{non} + \mathbf{D}_{ch}) \mathbf{E}^- \quad (11)$$

where the s^{th} post-FFT symbol obtained through the r^{th} ($r = 1, 2, \dots, N_R$) receiver antenna is denoted by $[\mathbf{M}_R]_{r,s}$, and we know

$$[\mathbf{E}^-]_{k,s} = N_S^{-1} e^{-j2\pi(s-1)(k-1)/N_S} \quad (12)$$

As in [28], we model the PA's nonlinear in-band distortion $\mathbf{D}_{non} \mathbf{E}^-$ as a Gaussian signal. The output of the M-QAM demodulator can be written as

$$\mathbf{U}_R = \mathbf{W} + \alpha \beta \mathbf{H} \mathbf{U} \quad (13)$$

where the sum of system impairments is denoted by \mathbf{W} , and the output symbol of the source bit stream is written as \mathbf{U} .

We write \mathbf{W} as

$$\mathbf{W} = (\alpha \mathbf{H} \mathbf{D}_{clip} + \mathbf{H} \mathbf{D}_{non} + \mathbf{D}_{ch}) \mathbf{E}^- \quad (14)$$

III. BFPA MODEL AND SNE/SER ANALYSIS

In subsection A, we present how we measure a PA chip and give the measurement results for building the PA model. And then in subsection B, we use the BA model to simplify the SNR analysis. Finally, we derive the SER performance in subsection C.

A. PA modeling and measurements

Numerous prior studies have extensively explored analytical models for nonlinear PAs in the literature. The power spectrum of PA's nonlinear distortion has been investigated in prior works like [29]. These works also established the relationship between the PA operating point and the signal SNR at the receiver antennas. However, they often involve complex calculations, including integrals and partial differentials, which hinder their practical applicability for extensive analysis of nonlinear PA systems. Some works also develop simple PA behavior models with consideration of memory effect [30]–[32]. However, the primary focus of this paper is to understand the impact of PA nonlinearity and clipping distortion. We are not interested in considering the memory effect, which brings additional computation complexity.

This paper utilizes a simple memoryless PA model known as the "BFPA model" to capture the PA nonlinearity. The concept of BFPA was developed in [33], comprehensively analyzed in [34], and then became widely used in later work like [9], [27], [28], [35], [36]. With the BFPA model, we focus on the analysis of the amplitude modulation to amplitude modulation (AM/AM) characteristic of the PA. By investigating this characteristic, we aim to understand the nonlinear behavior exhibited by the PA and its impact on system performance. The equivalent PA model is derived based on memoryless characteristics extracted from extensive laboratory measurements of the input-output behaviors of a commercially available PA. Fig. 2 presents the experimental setup employed for the PA measurement in this research.

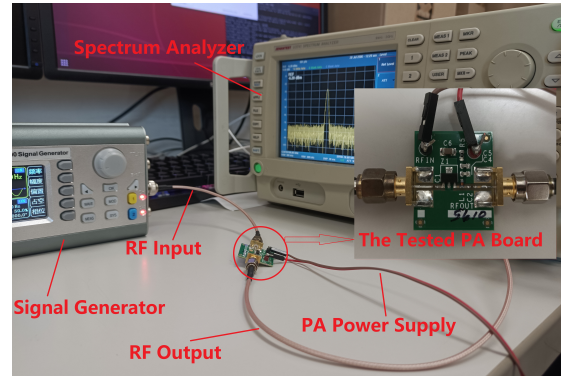


Figure 2. Experimental setup for the PA measurement.

We now explain our measurement as follows. We first generate a 2.4GHz single-tone signal with the signal generator. We then transmit the signal via the test PA and measure the PA's output with a spectrum analyzer. We keep testing different signal power and recording the PA's output power. Finally, we plot the scatter chart as in Fig. 3 and fit the AM-AM curve for the tested PA. For better illustration, we also present the ideal AM-AM curve for the tested PA by assuming that the PA is a linear one.

After the measurement, we use the fitted AM-AM curve to build the BFPA model as in [34]. Given a P -order BFPA model, let us denote the p^{th} order coefficients by b_p and denote the dynamic range of the model by P_{mod} .

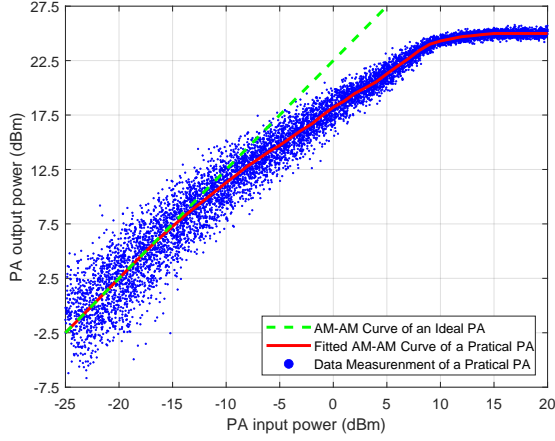


Figure 3. The scatter chart of the measured PA and the fitted AM-AM curve of the PA.

B. Polynomial Function of Receive SNR

Upon examination of the right side of (11), it is evident that the power of the desired signal can be further written as $\alpha^2 \beta^2 \|\mathbf{H}\|_F^2 E_U$. Additionally, the power of the impairment symbol \mathbf{W} is represented by E_W . Consequently, the SNR at the receiver, following the OFDM demodulator, can be represented as

$$\gamma = \frac{\alpha^2 \beta^2 \|\mathbf{H}\|_F^2 E_U}{E_W} \quad (15)$$

where E_W encompasses various sources of system distortion, including channel noise, signal clipping noise, and PA nonlinearity. In light of these considerations, we express it as

$$E_W = \sigma_{ch}^2 + \alpha^2 D_k E_U + \frac{1}{N_S} \sum_{t=1}^{N_T} \sum_{s=1}^{N_S} E \left([\mathbf{H} \mathbf{D}_{non} \mathbf{E}^-]_{t,s} \cdot [\mathbf{H} \mathbf{D}_{non} \mathbf{E}^-]_{t,s}^* \right) \quad (16)$$

[R3-5] We now delve into the modeling of PA nonlinearity to simplify the last term in (16). In this paper, we follow the IMP analysis presented in our previous paper [36] to approximate the power of PA's nonlinear distortion. Due to space limits, this paper does not repeat these derivation details. Instead, we present the outline of the derivation and refer our reader to [36] for detailed analysis and discussions. In general, the last term in (16) can be expressed as

$$\sum_{\delta=3,5,\dots} \sum_{s=1}^{N_S} \phi(\delta, s) \Omega(\delta, \beta^2 E_U) \quad (17)$$

where $\phi(\delta, s)$ denotes the number of δ order IMPs falling at the s^{th} OFDM subcarrier, and it can be counted through a numerical process [35]. Additionally, $\Omega(\eta, \beta^2 E_U)$ is the power of an individual δ order IMP, and it can be further written as

$$\Omega(\delta, \beta^2 E_U) = \left| \sum_{p=1}^P \left[b_p \cdot J_0^{N_S - \delta}(V_p) \cdot J_1^\delta(V_p) \right] \right|^2 \quad (18)$$

where J_{g_m} denote the g_m^{th} order Bessel function of the first kind, and b_p denotes the coefficients of a P -order BFPA model. Furthermore, V_p can be written as

$$V_p = \frac{2p\pi}{P_{mod} \sqrt{\beta^2 E_U / N_T N_S}} \quad (19)$$

where P_{mod} is the dynamic range of the P -order BFPA.

Further considering the range of the Bessel kernel and assuming $\delta = 1$, we have the power of a first-order IMP (i.e., the wanted signal) as

$$\Omega(1, \beta^2 E_U) = \frac{\beta^2 E_U}{N_T N_S} \left| \sum_{p=1}^P b_p \frac{p\pi}{P_{mod}} \right|^2 = \frac{a_1 \beta^2 E_U}{N_T N_S} \quad (20)$$

where

$$a_1 = \left| \sum_{p=1}^P \left(\frac{b_p p\pi}{P_{mod}} \right) \right|^2 \quad (21)$$

Given that the domination of PA's nonlinear distortion comes from the third-order IMPs, we have

$$\begin{aligned} \sum_{\delta=3,5,\dots} \Omega(\eta, \beta^2 E_U) &\approx \Omega(3, \beta^2 E_U) \\ &= \left(\frac{\beta^2 E_U}{N_T N_S} \right)^3 \left| \sum_{p=1}^P b_p \left(\frac{p\pi}{P_{mod}} \right)^3 \right|^2 = \frac{a_3 \beta^6}{N_T^3 N_S^3} E_U^3 \end{aligned} \quad (22)$$

where

$$a_3 = \left| \sum_{p=1}^P b_p \left(\frac{p\pi}{P_{mod}} \right)^3 \right|^2 \quad (23)$$

With a similar analysis, we have the clipping distortion as

$$\begin{aligned} \alpha^2 D_k E_U &= \Omega(1, D_k E_U) \\ &= \frac{D_k E_U}{N_T N_S} \left| \sum_{p=1}^P b_p \frac{p\pi}{P_{mod}} \right|^2 = \frac{a_1 D_k}{N_T N_S} E_U \end{aligned} \quad (24)$$

Now, with (16), (20), (22), and (24), we reconsider the equation in 15 and obtain the receiver SNR in a polynomial form, which is

$$\gamma = \frac{a_1 \beta^2 \|\mathbf{H}\|_F^2 E_U}{\sigma_{ch}^2 + \frac{a_1 D_k}{N_T N_S} E_U + \sum_{s=1}^{N_S} \phi(3, s) \cdot \frac{a_3 \beta^6}{N_T^3 N_S^3} E_U^3} \quad (25)$$

C. System SER

From [37], it is established that the receiver SNR's probability distribution function (PDF) is given by

$$P_e(\gamma) = \|\mathbf{H}\|_F^2 e^{-\|\mathbf{H}\|_F^2 / \gamma} / \Gamma(\lambda) \quad (26)$$

where

$$\lambda = E \left(\|\mathbf{H}\|_F^2 \right) = N_T \cdot N_S \quad (27)$$

and $\Gamma(z)$ represents the Gamma function, which can be expressed as

$$\Gamma(z) = \int_0^\infty x^{z-1} e^{-x} dx \quad (28)$$

After being captured at the receiver antennas and processed by the spatial stream parser, received symbols are inputted

into the M-QAM decision block. As has been established in reference [38], the relationship between the receiver SNR and the symbol estimation error probability can be expressed as

$$P_w(\gamma) = \frac{4(\sqrt{M}-1)}{\pi\sqrt{M}} \int_0^{\frac{\pi}{2}} \left(\frac{\sin^2\theta}{\sin^2\theta + g_{QAM}\gamma} \right)^{N_R} d\theta \\ - \frac{4}{\pi} \left(\frac{\sqrt{M}-1}{\sqrt{M}} \right)^2 \int_0^{\frac{\pi}{2}} \left(\frac{\sin^2\theta}{\sin^2\theta + g_{QAM}\gamma} \right)^{N_R} d\theta \quad (29)$$

where

$$g_{QAM} = \frac{3}{2(M-1)} \quad (30)$$

Hence, the SER of a nonlinear OFDM system with clipping can be written as

$$SER(\gamma) = \int_0^\infty P_e(\gamma)P_w(\gamma)d\gamma \\ \approx \left(\frac{\sqrt{M}-1}{\pi\sqrt{M}} \right) \int_0^{\pi/2} \int_0^\infty \frac{4}{\gamma} e^{-\left(\frac{3\gamma}{2\sin^2\theta(M-1)} + \|\mathbf{H}\|_F^2\right)} d\gamma d\theta \quad (31) \\ = 2 \frac{\sqrt{M}-1}{\pi\sqrt{M}} \left(\frac{2(M-1)\|\mathbf{H}\|_F^2}{3\gamma} \right)^\lambda B\left(\lambda + \frac{1}{2}, \frac{1}{2}\right) \\ \cdot F_1\left(\lambda, \lambda + \frac{1}{2}, \lambda + 1, -\frac{2(M-1)\|\mathbf{H}\|_F^2}{3\gamma}\right)$$

where $B(x, y) = \int_0^1 t^{x-1}(1-t)^{y-1}dt$ is Beta function, and $F_1(a, b, c, d)$ denotes the well known Gaussian hypergeometric function [39].

At the end of this section, we would like to re-emphasize the complexity of the SNR expression and the SER expression presented in (25) and (31), respectively. The complexity of these two expressions is simplified from two aspects. First, we remove the lengthy expressions about memory effects, given that we mainly focus on the nonlinearity of the amplifier. Second, as we have discussed in Subsection A, the application of the BFPA model significantly reduces the complexity of our IMP analysis. These efforts simplify the expressions of SER and SNR, which facilitates the following analysis and optimization.

IV. SER OPTIMIZATION

Section III gives the SER of the studied system in (31), while this section further optimizes the SER in different scenarios.

Before technical details, we give an outline of the following three subsections and make the following notations. Subsection A assumes a constant η and optimizes the system operating point. The optimal SNR, the optimal, system operating point, and the optimal SER performance are denoted as $\gamma_{E_U}^{opt}$, E_U^{opt} , and $SER_{E_U}^{opt}$, respectively. Subsection B assumes a constant E_U and optimizes the signal clipping level. We denote the optimal signal clipping level, the optimal SNR, and the optimal SER as η^{opt} , γ_η^{opt} , and SER_η^{opt} , respectively. Subsection C undertakes the joint optimization of E_U (power

of the desired signal) and η (signal clipping level). The optimal signal clipping level and the optimal PA operating point are denoted by η^g and E_U^g , respectively, where the superscript g represents the global optimum. The resulting optimal values for the SNR and SER are denoted as γ^g and SER^g , respectively.

A. Optimization of PA Operation Point

From (31), we can derive the function for the SER with respect to the receiver SNR. The resulting expression is presented as (32) on the following page.

Furthermore, with(32), we have

$$\frac{\partial}{\partial\gamma} F_1\left(\lambda, \lambda + \frac{1}{2}, \lambda + 1, -\frac{2(M-1)\|\mathbf{H}\|_F^2}{3\gamma}\right) > 0 \quad (33)$$

Since $\partial SER(\gamma)/\partial\gamma$ is negative, we know SER is a decreasing function of γ . In other words, to obtain the minimum SER, we need to find the maximum possible SNR.

We now look at how to find $\gamma_{E_U}^{opt}$. With the expression in (17), we obtain the partial derivation function of $\gamma(\eta, E_U)$ as the respect of E_U as

$$\frac{\partial\gamma}{\partial E_U} = \frac{a_1\beta^2\|\mathbf{H}\|_F^2\left(\sigma_{ch}^2 - \frac{2a_3\Phi\beta^6}{N_T^3N_S^4}E_U^3\right)}{\left(\frac{a_1D_k}{N_TN_S}E_U + \frac{a_3\beta^6\Phi}{N_T^3N_S^4}E_U^3 + \sigma_{ch}^2\right)^2} \quad (34)$$

From (34), we know that

$$\frac{\partial\gamma}{\partial E_U} \begin{cases} > 0, E_U < \frac{N_TN_S^{4/3}}{\beta^2} \sqrt[3]{\frac{\sigma_{ch}^2}{2a_3\Phi}} \\ = 0, E_U = \frac{N_TN_S^{4/3}}{\beta^2} \sqrt[3]{\frac{\sigma_{ch}^2}{2a_3\Phi}} \\ < 0, E_U > \frac{N_TN_S^{4/3}}{\beta^2} \sqrt[3]{\frac{\sigma_{ch}^2}{2a_3\Phi}} \end{cases} \quad (35)$$

As we can see from (35), $\partial\gamma/\partial E_U$ turns from positive to negative with the increase of E_U . Therefore, when $\partial\gamma/\partial E_U = 0$, γ reaches its maximum value $\gamma_{E_U}^{opt}$, and the corresponding E_U can be written as

$$E_U^{opt} = \frac{N_TN_S^{\frac{4}{3}}}{\beta^2} \sqrt[3]{\frac{\sigma_{ch}^2}{2a_3\Phi}} \quad (36)$$

Introducing (36) into (17), we have

$$\gamma_{E_U}^{opt} = \frac{a_1\beta^2N_TN_S^{4/3}\|\mathbf{H}\|_F^2(2a_3\Phi)^{-1/3}\sigma_{ch}^{2/3}}{a_1N_S^{1/3}D_k(2a_3\Phi)^{-1/3}\sigma_{ch}^{2/3} + 2\beta^2\sigma_{ch}^2} \quad (37)$$

Introducing (37) to (31), the optimal SER performance can be written as

$$SER_{E_U}^{opt} = 2 \frac{\sqrt{M}-1}{\pi\sqrt{M}} \cdot \left(\frac{2(M-1)\|\mathbf{H}\|_F^2}{3\gamma_{E_U}^{opt}} \right)^\lambda \\ B\left(\lambda + \frac{1}{2}, \frac{1}{2}\right) \cdot F_1\left(\lambda, \lambda + \frac{1}{2}, \lambda + 1, -\frac{2(M-1)\|\mathbf{H}\|_F^2}{3\gamma_{E_U}^{opt}}\right) \quad (38)$$

$$\frac{\partial SER}{\partial \gamma} = -2 \frac{\sqrt{M}-1}{\pi\sqrt{M}} \cdot B\left(\lambda + \frac{1}{2}, \frac{1}{2}\right) \left\{ \begin{aligned} & \frac{2\lambda(M-1)\|\mathbf{H}\|_F^2}{3\gamma^2} \left(\frac{2(M-1)\|\mathbf{H}\|_F^2}{3\gamma} \right)^{\lambda-1} \\ & \cdot F_1\left(\lambda, \lambda + \frac{1}{2}, \lambda + 1, -\frac{2(M-1)\|\mathbf{H}\|_F^2}{3\gamma}\right) \\ & + \left(\frac{2(M-1)\|\mathbf{H}\|_F^2}{3\gamma} \right)^\lambda \frac{\partial F_1\left(\lambda, \lambda + \frac{1}{2}, \lambda + 1, -\frac{2(M-1)\|\mathbf{H}\|_F^2}{3\gamma}\right)}{\partial \gamma} \end{aligned} \right\} \quad (32)$$

B. Optimization of Signal Clipping Level

We see from (5) that the derivation function of power scaling factor β with respect to η should be written as

$$\frac{\partial \beta}{\partial \eta} = \int_{\eta}^{\infty} e^{-t^2} dt + \eta e^{-\eta^2} > 0 \quad (39)$$

From (39), we know that the power scaling factor β is a monotone increasing function of η . We are interested in finding the optimal β so that we can do a simple mapping to obtain the optimal η .

The partial derivation function for γ with respect to β^2 can be calculated as

$$\frac{\partial \gamma}{\partial \beta^2} = \frac{\left(\frac{a_1 D_k E_U}{N_T N_S} + \sigma_{ch}^2 - \frac{2a_3 \Phi E_U^3}{N_T^3 N_S^4} \beta^6 \right) a_1 \|\mathbf{H}\|_F^2 E_U}{\left(\frac{a_1 D_k E_U}{N_T N_S} + \frac{a_3 \beta^6 \Phi E_U^3}{N_T^3 N_S^4} + \sigma_{ch}^2 \right)^2} \quad (40)$$

Let (40) be zero. We note that the optimal power scaling factor can be calculated through the following equation:

$$\frac{\partial \gamma}{\partial \beta^2} = 0 \Leftrightarrow -\frac{2a_3 \Phi E_U^3}{N_T^3 N_S^4} \beta^6 + \frac{a_1 D_k E_U}{N_T N_S} + \sigma_{ch}^2 = 0 \quad (41)$$

Further consider $0 < \beta^2 < 1$, the only solution of (41) can be written as

$$\beta^2 = \frac{N_S N_T^{\frac{2}{3}}}{E_U} \sqrt[3]{\frac{(a_1 D_k E_U + \sigma_{ch}^2)}{2a_3 \Phi}} \quad (42)$$

With (42), it can be proved that

$$\frac{\partial \gamma}{\partial \beta^2} \begin{cases} > 0, 0 < \beta^2 < \frac{N_S N_T^{\frac{2}{3}}}{E_U} \sqrt[3]{\frac{(a_1 D_k E_U + \sigma_{ch}^2)}{2a_3 \Phi}} \\ = 0, \beta^2 = \frac{N_S N_T^{\frac{2}{3}}}{E_U} \sqrt[3]{\frac{(a_1 D_k E_U + \sigma_{ch}^2)}{2a_3 \Phi}} \\ < 0, \beta^2 > \frac{N_S N_T^{\frac{2}{3}}}{E_U} \sqrt[3]{\frac{(a_1 D_k E_U + \sigma_{ch}^2)}{2a_3 \Phi}} \end{cases} \quad (43)$$

We see from (43) that $\partial \gamma / \partial \beta^2$ changes from positive to negative with the growing up of β^2 . As a result, there is an optimal signal clipping level η^{opt} that can result in the maximum γ . With (43) and (5), we can then calculate η^{opt} as

$$\eta^{opt} = \ln \left(\sqrt{1 - \sqrt{\frac{N_S N_T^{\frac{2}{3}}}{E_U} \sqrt[3]{\frac{(a_1 D_k E_U + \sigma_{ch}^2)}{2a_3 \Phi}}}} \right) \quad (44)$$

We already know from subsection A that SER is a decreasing function of receiver SNR. Hence, we substitute (44) into (31) and obtain the optimal SER as

$$SER_{\eta}^{opt} = 2 \frac{\sqrt{M}-1}{\pi\sqrt{M}} \cdot \left(\frac{2(M-1)\|\mathbf{H}\|_F^2}{3\gamma_{\eta}^{opt}} \right)^\lambda B\left(\lambda + \frac{1}{2}, \frac{1}{2}\right) \cdot F_1\left(\lambda, \lambda + \frac{1}{2}, \lambda + 1, -\frac{2(M-1)\|\mathbf{H}\|_F^2}{3\gamma_{\eta}^{opt}}\right) \quad (45)$$

Then, we see that the optimal SNR can be written as

$$\gamma_{\eta}^{opt} = \frac{a_1 \beta_{opt}^2 \|\mathbf{H}\|_F^2 E_U}{\frac{a_3 \beta_{opt}^6 \Phi E_U^3}{N_T^3 N_S^4} + \frac{a_1 D_k E_U}{N_T N_S} + \sigma_{ch}^2} \quad (46)$$

C. Joint Optimization

The derivation function of $\gamma(\eta, E_U)$ is

$$\begin{aligned} \frac{\partial^2 \gamma}{\partial \beta \partial E_U} &= \frac{\partial^2}{\partial \beta \partial E_U} \left(\frac{a_1 \beta^2 \|\mathbf{H}\|_F^2 E_U}{\frac{a_1 D_k E_C}{N_T N_S} + \frac{a_3 \beta^6 \Phi E_U^3}{N_T^3 N_S^4} + \sigma_{ch}^2} \right) \\ &= \frac{\partial}{\partial E_U} \left(\frac{a_1 (\beta^g)^2 \|\mathbf{H}\|_F^2 E_U}{\frac{a_1 D_k E_C}{N_T N_S} + \frac{a_3 (\beta^g)^6 \Phi E_U^3}{N_T^3 N_S^4} + \sigma_{ch}^2} \right) \\ &= \frac{a_1 (\beta^g)^2 \|\mathbf{H}\|_F^2 \sigma_{ch}^2 - \frac{2a_1 a_3 (\beta^g)^8 \|\mathbf{H}\|_F^2 \Phi E_U^3}{N_T^3 N_S^4}}{\left(\frac{a_1 D_k E_C}{N_T N_S} + \frac{a_3 (\beta^g)^6 \Phi E_U^3}{N_T^3 N_S^4} + \sigma_{ch}^2 \right)^2} \end{aligned} \quad (47)$$

where β^g is the optimal signal power scaling factor that can result in η^g .

Substituting (5) to (47) and letting $\frac{\partial^2 \gamma}{\partial \beta \partial E_U} = 0$, we have

$$E_U^g = \frac{N_S^2 - \sigma_{ch}^2}{a_1 D_k} \quad (48)$$

$$\eta^g = \ln \left(\sqrt{1 - \sqrt{\frac{a_1 D_k N_T N_S^{\frac{4}{3}} \sqrt[3]{\frac{\sigma_{ch}^2}{2a_3 \Phi}}}{N_S^2 - \sigma_{ch}^2}}} \right) \quad (49)$$

With (17), (31), (48) and (49), we obtain SER^g and γ^g as (50) and (51) presented in the next page.

V. SIMULATIONS AND DISCUSSIONS

At the beginning of this section, we explain why the increase in the number of subcarriers makes PA's nonlinearity a more challenging problem. Here we focus on a linear OFDM system's complementary cumulative distribution function (CCDF), which represents the probability of the system's

$$SER^g = \frac{2(\sqrt{M} - 1)}{\pi\sqrt{M}} \cdot \left(\frac{2(M-1) \|\mathbf{H}\|_F^2}{3\gamma^g} \right)^\lambda B\left(\lambda + \frac{1}{2}, \frac{1}{2}\right) \cdot F_1\left(\lambda, \lambda + \frac{1}{2}, \lambda + 1, -\frac{2(M-1) \|\mathbf{H}\|_F^2}{3\gamma^g}\right) \quad (50)$$

$$\gamma^g = \frac{N_T N_S \|\mathbf{H}\|_F^2 \Omega\left(1, N_T N_S^{4/3} \sqrt[3]{\frac{\sigma_{ch}^2}{2a_3\Phi}}\right)}{N_S^{-1} \Omega\left(3, N_T N_S^{4/3} \sqrt[3]{\frac{\sigma_{ch}^2}{2a_3\Phi}}\right) \sum_{s=1}^{N_S} \phi(3, s) + \Omega\left(1, \frac{N_S^2 - \sigma_{ch}^2}{a_1}\right) + \sigma_{ch}^2} \quad (51)$$

actual PAPR exceeding a targeted PAPR threshold [40]. As we can see from Fig. 4, given the same PAPR threshold (say 9dB), OFDM systems with larger N_S have significantly higher CCDFs. In this regard, with the rapid increase of N_S , modern wireless communication systems have much higher CCDF than before, making the OFDM system more sensitive to PA's nonlinearity. The above observation justifies the motivation of considering nonlinear amplifiers in this research.

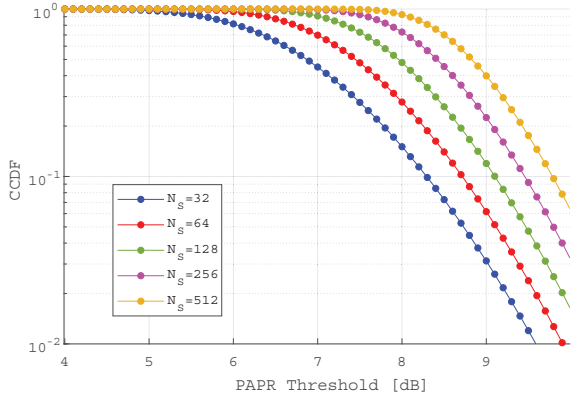


Figure 4. How the system's CCDF changes with PAPR under different subcarrier numbers. For detailed explanations about how CCDF is defined and calculated, we refer readers to Section III of [40].

The rest of this section validates our analytical results by simulating the studied OFDM system with signal clipping distortion and PA nonlinear distortion. We then study how the number of antennas affects the system's SER performance and examine the total degradation (TD) performance of the system.

In the following simulations, we set N_S as 64, which corresponds to the length of the OFDM modulator/demodulator block. The over-sampling rate of the OFDM symbols is set to 4. Furthermore, unless stated otherwise, we consider a MIMO configuration with a 2×2 antenna setting and employ 4-QAM as the default modulation scheme. We assume that the quasi-static Rayleigh channel is normalized, and we refer readers to [41] for implementation details of the channel.

Fig. 5, Fig. 6, and Fig. 7 are presented to examine the influence of the PA operating point E_U on the SER performance under various system configurations while keeping η constant. These figures provide a comprehensive understanding of the relationship between E_U and SER, with a comparison of simulated and analytical curves.

In Fig. 5, it is evident that each nonlinear case exhibits an

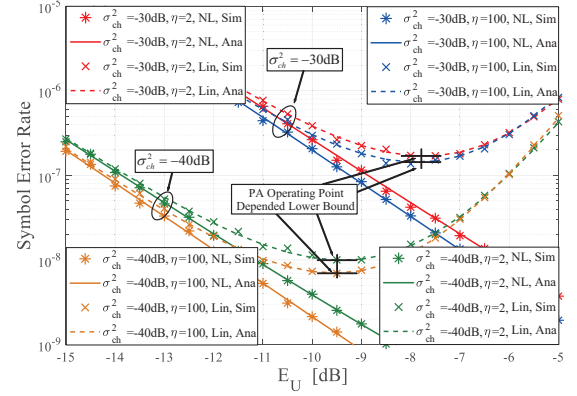


Figure 5. How SER changes with E_U under different noise and clipping settings. Both simulated (Sim) and analytical (Ana) results consider two different assumptions: nonlinear (NL) PAs and linear (Lin) PA.

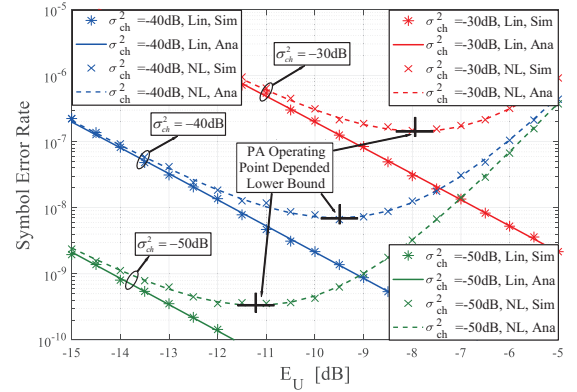


Figure 6. The influence of channel noise under different E_U . Here we let $\eta = 100$. Both simulated (Sim) and analytical (Ana) results consider two different assumptions: nonlinear (NL) PAs and linear (Lin) PAs.

SER lower bound that is dependent on E_U . This phenomenon can be explained as follows: when E_U is not large, the PA stays in its linear region, hence its nonlinearity could be negligible. The increase of E_U raises the PA's input power and leads to a higher SNR and a lower SER. However, when E_U is increased beyond a certain point, further increasing it results in very high nonlinear distortion. An SER lower bound can be observed when the detrimental effect of nonlinear distortion counteracts the amplification of the desired signal. Here the PA's operating point that results in this SER lower bound is denoted as E_U^{opt} . Beyond E_U^{opt} , further increase E_U deteriorates the SER performance.

From Fig. 6, we can see that the lower bound of system

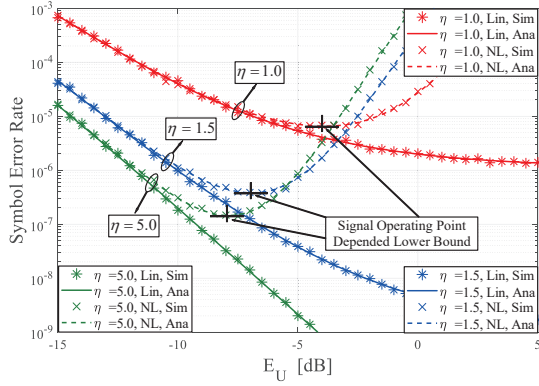


Figure 7. The influence of signal clipping level under different E_U . Here we let channel noise be -30dB . Both simulated (Sim) and analytical (Ana) results are presented.

SER and E_U^{opt} is positively correlated with σ_{ch}^2 , the channel noise. This is, a higher noise level necessitates a higher E_U to reach the optimal SER, but the resulting SER lower bound will be larger compared to scenarios with lower noise levels. Furthermore, Fig. 7 demonstrates a negative relationship between E_U^{opt} , the SER lower bound, and η , the clipping level.

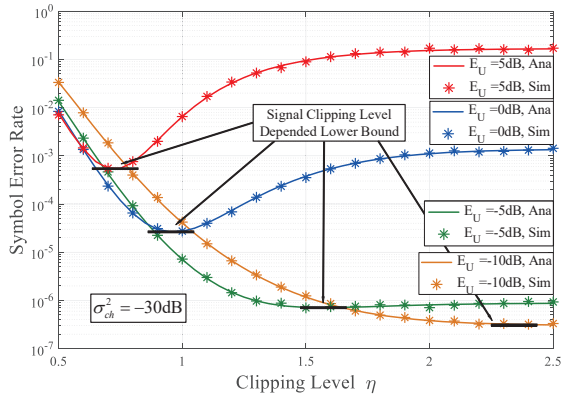


Figure 8. The performance of SER as a function of signal clipping level η when nonlinear PAs are considered. Both analytical (Ana) and simulated (Sim) results are presented.

Fig. 8 investigates η 's impact on the SER when E_U is constant. Both analytical and simulated SER curves are presented, considering the presence of significant nonlinear distortion in the PA. Notably, each curve exhibits an SER lower bound that is clipping level-dependent. When the PA operating point is sufficiently high, such as $E_U = 5\text{ dB}$ or 0 dB , increasing the clipping level initially leads to a decrease in SER. This is because signal clipping can help mitigate the nonlinear distortion of a PA by reducing the signal's PAPR. However, further, increasing η beyond the optimal value can result in significant degradation of the system's SER performance because clipping noise now dominates the system's impairment.

In Fig. 9, we treat SER as a function of both PA operating point E_U and the signal clipping level η , with a consideration of nonlinear PAs. As anticipated in Section IV, we can observe a global optimal SER in the figure. Specifically, when the

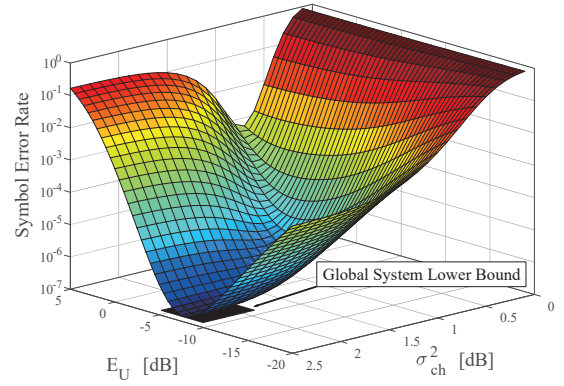


Figure 9. A 3D figure showing the relationship between 1) system SER, 2) signal clipping level η , and 3) PA operating point E_U . Channel noise $\sigma_{ch}^2 = -30\text{dB}$. Nonlinear PAs are considered.

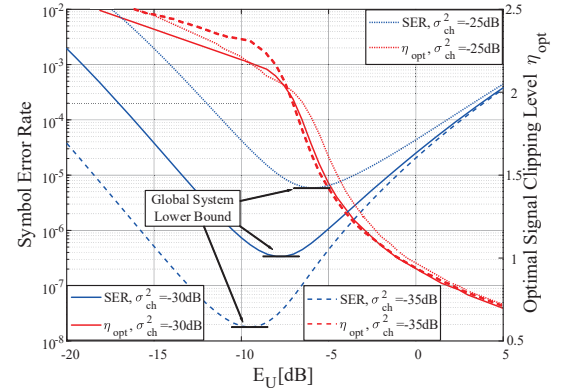


Figure 10. How the curves of SER performance and the curves of η_{opt} optimal signal clipping level change according to the system operating point E_U .

channel noise σ_{ch}^2 is set to -30 dB , the global optimal SER is determined to be 8.57×10^{-6} , which aligns precisely with the simulated results.

Fig. 10 presents how SER and the optimal signal clipping level change with the system operating point E_U under various noise conditions. It can be seen that there is a global system lower bound of SER when system operating point E_U sweeps. Moreover, the optimal signal clipping level η_{opt} is a convex function, where its convex point corresponds to the system operating point. Besides, the global system lower bound is positively related to the channel noise σ_{ch}^2 , and the global system lower bound of SER is also positively related to σ_{ch}^2 . This can be explained by (51): γ^g is positively related to the channel noise.

Fig. 11 presents how the number of transmit/receive antennas affects the system SER when nonlinear amplifiers are considered. As the figure shows, using more transmit/receive antennas can significantly reduce the system's SER, although it comes with increased system complexity.

Fig. 12 presents an investigation into the relationship between the PA output back off (OBO) and the overall system TD. The OBO refers to the reduction in output power from the PA's maximum allowed output power, indicating the extent to which the PA operates in its nonlinear region. On the other

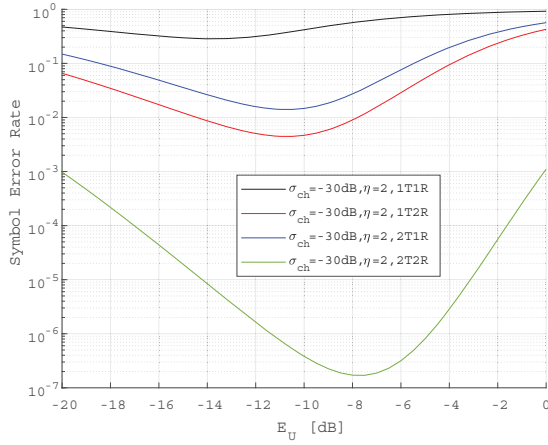


Figure 11. How SER changes with E_U under different numbers of transmit/receive antennas. In the figure, $nTmR$ refers to a system with n transmit antennas plus m receive antennas.

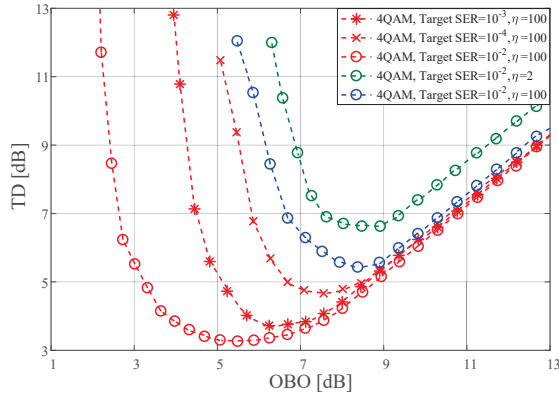


Figure 12. TD performance when various target SERs and different η values are considered.

hand, TD represents the SNR loss compared to that of an ideal linear amplifier in achieving a specific level of SER. For each target SER, the TD graphs in Fig. 12 exhibit a truncation point in the low-value OBO range, with the associated SER lower bound being equal to the target SER. Notably, as the PA operates within its highly nonlinear range, the TD graphs noticeably deviate from those obtained with a linear PA. It is understandable that as the target SER decreases, the OBO value at which the truncation point occurs increases. This trend becomes evident when examining the TD graph for 4-QAM signals, particularly when the target SER ranges from 10^{-2} to 10^{-4} . Furthermore, a decrease in the parameter η leads to an increase in the OBO value. This observation is apparent when analyzing the TD graph for 4-QAM signals with varying η values from 100 to 2.

VI. CONCLUSION

This paper studies the performance of OFDM systems with considerations of signal clipping distortion and PA nonlinearity distortion. By modeling the PA and analyzing its IMPs, we derive the system SNR and SER in a polynomial form. These derivations offer the advantage of low complexity while maintaining reasonable accuracy. Additionally, we conduct joint

optimization of the clipping distortion and the PA nonlinearity to obtain the global minimum SER. This optimization process identifies the optimal signal clipping level and the optimal PA operating point. Furthermore, we examine the influence of system parameters on the SER performance under various configurations.

REFERENCES

- [1] Y. Du, L. Hao, and Y. Lei, "SER analysis and joint optimization in nonlinear MIMO-OFDM systems with clipping," in *IEEE Vehicular Technology Conference (VTC-Spring)*, 2023.
- [2] R. Yoshizawa and H. Ochiai, "Energy efficiency improvement of coded OFDM systems based on PAPR reduction," *IEEE Syst. J.*, vol. 11, no. 2, pp. 717–728, 2017.
- [3] P. Aggarwal and V. A. Bohara, "End-to-end theoretical evaluation of a nonlinear MIMO-OFDM system in the presence of digital predistorter," *IEEE Syst. J.*, vol. 13, no. 3, pp. 2309–2319, 2019.
- [4] M. Cherif, A. Arfaoui, R. Zayani, and R. Bouallegue, "End-to-end deep learning for multipair two-way massive MIMO with PA impairments," *IEEE Syst. J.*, vol. 17, no. 2, pp. 3150–3159, 2023.
- [5] P. Aggarwal, A. Pradhan, and V. A. Bohara, "A downlink multiuser MIMO-OFDM system with nonideal oscillators and amplifiers: Characterization and performance analysis," *IEEE Syst. J.*, vol. 15, no. 1, pp. 715–726, 2021.
- [6] P. Priya and D. Sen, "Data detection with CFO uncertainty and nonlinearity for mmWave MIMO-OFDM systems," *IEEE Syst. J.*, vol. 16, no. 3, pp. 3734–3745, 2022.
- [7] B. Adebisi, K. Anoh, and K. M. Rabie, "Enhanced nonlinear companding scheme for reducing PAPR of OFDM systems," *IEEE Syst. J.*, vol. 13, no. 1, pp. 65–75, 2019.
- [8] P. Naveen and P. Jena, "Adaptive protection scheme for microgrid with multiple point of common couplings," *IEEE Syst. J.*, vol. 15, no. 4, pp. 5618–5629, 2021.
- [9] Y. Du, L. Hao, and Y. Lei, "SER optimization in OFDM-IM systems with nonlinear power amplifiers," *IEEE Trans. Veh. Technol.*, pp. 1–6, 2023.
- [10] Y. Du, S. C. Liew, and Y. Shao, "Efficient FFT computation in IFDMA transceivers," *IEEE Trans. Wirel. Commun.*, pp. 1–11, 2023.
- [11] S. Gokceli, T. Levanen, T. Riihonen, M. Renfors, and M. Valkama, "Frequency-selective PAPR reduction for OFDM," *IEEE Trans. Veh. Technol.*, vol. 68, no. 6, pp. 6167–6171, 2019.
- [12] S. Y. Zhang and B. Shahrava, "A SLM scheme for PAPR reduction in polar coded OFDM-IM systems without using side information," *IEEE Trans. Broadcast.*, pp. 1–10, 2020.
- [13] Seung Hee Han and Jae Hong Lee, "An overview of peak-to-average power ratio reduction techniques for multicarrier transmission," *IEEE Wireless Commun.*, vol. 12, no. 2, pp. 56–65, 2005.
- [14] J. Chen and C. Wen, "PAPR reduction of OFDM signals using cross-entropy-based tone injection schemes," *IEEE Signal Process. Lett.*, vol. 17, no. 8, pp. 727–730, 2010.
- [15] K. Bae, J. G. Andrews, and E. J. Powers, "Adaptive active constellation extension algorithm for peak-to-average ratio reduction in OFDM," *IEEE Commun. Lett.*, vol. 14, no. 1, pp. 39–41, 2010.
- [16] S. C. Thompson, J. G. Proakis, and J. R. Zeidler, "The effectiveness of signal clipping for PAPR and total degradation reduction in OFDM systems," in *IEEE Global Telecommunications Conference (GLOBECOM)*, vol. 5, 2005.
- [17] H. Saedi, M. Sharif, and F. Marvasti, "Clipping noise cancellation in OFDM systems using oversampled signal reconstruction," *IEEE Commun. Lett.*, vol. 6, no. 2, pp. 73–75, 2002.
- [18] D. Guel and J. Palicot, "Clipping formulated as an adding signal technique for OFDM peak power reduction," in *IEEE Vehicular Technology Conference (VTC-Spring)*, 2009.
- [19] S. Gokceli, T. Levanen, T. Riihonen, M. Renfors, and M. Valkama, "Frequency-selective PAPR reduction for OFDM," *IEEE Trans. Veh. Technol.*, vol. 68, no. 6, pp. 6167–6171, 2019.
- [20] A. Ali, A. Al-Rabah, M. Masood, and T. Y. Al-Naffouri, "Receiver-based recovery of clipped OFDM signals for PAPR reduction: A bayesian approach," *IEEE Access*, vol. 2, pp. 1213–1224, 2014.
- [21] J. Armstrong, "Peak-to-average power reduction for OFDM by repeated clipping and frequency domain filtering," *Electron. Lett.*, vol. 38, no. 5, pp. 246–247, 2002.

- [22] K. Anoh, C. Tanriover, and B. Adebisi, "On the optimization of iterative clipping and filtering for PAPR reduction in OFDM systems," *IEEE Access*, vol. 5, pp. 12 004–12 013, 2017.
- [23] K. Anoh, C. Tanriover, B. Adebisi, and M. Hammoudeh, "A new approach to iterative clipping and filtering PAPR reduction scheme for OFDM systems," *IEEE Access*, vol. 6, pp. 17 533–17 544, 2018.
- [24] I. Sohn and S. C. Kim, "Neural network based simplified clipping and filtering technique for PAPR reduction of OFDM signals," *IEEE Commun. Lett.*, vol. 19, no. 8, pp. 1438–1441, 2015.
- [25] L. Yang, K. Song, and Y. M. Siu, "Iterative clipping noise recovery of OFDM signals based on compressed sensing," *IEEE Trans. Broadcast.*, vol. 63, no. 4, pp. 706–713, 2017.
- [26] A. A. Eltholth, A. R. Mekhail, A. Elshirbini, M. Dessouki, and A. Abdelfattah, "Modeling the effect of clipping and power amplifier nonlinearities on OFDM systems," *Ubiquitous Comput. Commun. J.*, vol. 3, no. 1, pp. 54–59, 2009.
- [27] L. Yiming, M. O'Droma, and J. Ye, "A practical analysis of performance optimization in OSTBC based nonlinear MIMO-OFDM systems," *IEEE Trans. Commun.*, vol. 62, no. 3, pp. 930–938, 2014.
- [28] Y. Du, Y. Lei, and S. McGrath, "SER optimization in transparent OFDM relay systems in the presence of dual nonlinearity," *Digit. Signal Process.*, vol. 126, p. 103506, 2022.
- [29] H. Hemesi, A. Abdipour, and A. Mohammadi, "Analytical modeling of MIMO-OFDM system in the presence of nonlinear power amplifier with memory," *IEEE Trans. Commun.*, vol. 61, no. 1, pp. 155–163, 2013.
- [30] A. A. Saleh, "Frequency-independent and frequency-dependent nonlinear models of TWT amplifiers," *IEEE Trans Commun.*, vol. 29, no. 11, pp. 1715–1720, 1981.
- [31] P. Asbeck, H. Kobayashi, M. Iwamoto, G. Hanington, S. Nam, and L. Larson, "Augmented behavioral characterization for modeling the nonlinear response of power amplifiers," in *IEEE MTT-S International Microwave Symposium Digest*, vol. 1, 2002.
- [32] P. Draxler, I. Langmore, T. Hung, and P. Asbeck, "Time domain characterization of power amplifiers with memory effects," in *IEEE MTT-S International Microwave Symposium Digest*, vol. 2, 2003.
- [33] Y. Lei and M. O'Droma, "Behavioural analysis of internal mechanism of nonlinear distortion in OFDM signal systems," in *2009 IEEE Global Telecommunications Conference*, 2009, pp. 1–5.
- [34] M. O'Droma and L. Yiming, "A new Bessel-Fourier memoryless nonlinear power amplifier behavioral model," *IEEE Microw. Wirel. Compon. Lett.*, vol. 23, no. 1, pp. 25–27, 2013.
- [35] Y. Du, J. Chen, Y. Lei, and X. Hao, "Performance analysis of nonlinear spatial modulation multiple-input multiple-output systems," *Digit. Signal Process.*, vol. 115, p. 103064, 2021.
- [36] L. Yiming and M. O'Droma, "A novel decomposition analysis of nonlinear distortion in OFDM transmitter systems," *IEEE Trans. Signal Process.*, vol. 63, no. 19, pp. 5264–5273, 2015.
- [37] H. Zhao, Y. Gong, Y. L. Guan, and S. Li, "Performance analysis of space-time block codes in Nakagami-m keyhole channels with arbitrary fading parameters," in *2008 IEEE International Conference on Communications*, 2008, pp. 4090–4094.
- [38] A. Goldsmith, *Wireless Communications*. Cambridge University Press, 2005.
- [39] M. Abramowitz, I. A. Stegun, and R. H. Romer, "Handbook of mathematical functions with formulas, graphs, and mathematical tables," 1988.
- [40] S. P. Yadav and S. C. Bera, "PAPR reduction using clipping and filtering technique for nonlinear communication systems," in *IEEE International Conference on Computing, Communication & Automation*, 2015.
- [41] MathWorks, *Communication Toolbox*, 2024. [Online]. Available: <https://www.mathworks.com/help/comm/ref/comm-rayleighchannel-system-object.html>